Journal of Superconductivity and Novel Magnetism (2022) 35:3371–3378
https://doi.org/10.1007/s10948-022-06362-x

ORIGINAL PAPER

Magnetic and Photocatalytic Activity of Pure $BaFe_{12}O_{19}$ and $BaFe_{12}O_{19}$-TiO_2 Hexagonal Ferrite Nanocomposites

Olfa khemakhem[1,2] · Jamila Ben Naceur[2] · Firas Ayadi[3] · Wissem Cheikhrouhou-Koubaa[1] · Mohamed Koubaa[1] · Virginie Nachbaur[3] · Radhouane Chtourou[2] · Abdelwaheb Cheikhrouhou[1]

Received: 25 June 2022 / Accepted: 27 July 2022 / Published online: 9 August 2022
© The Author(s), under exclusive licence to Springer Science+Business Media, LLC, part of Springer Nature 2022

Abstract
Hard hexagonal barium ferrite $BaFe_{12}O_{19}$ (BaM), as well as core–shell structure $BaFe_{12}O_{19}$-TiO_2 composite nanoparticles, was successfully prepared by solid state reaction. An interesting photocatalytic activity has been noticed for the first time in pure BaM and doped TiO_2 nanopowders. The obtained powders can photodegrade organic pollutants in the dispersion system effectively and can be recycled easily using a magnetic field. The $BaFe_{12}O_{19}$-TiO_2 magnetic photocatalyst is composed of two parts: (1) TiO_2 shell used for photocatalysis and (2) $BaFe_{12}O_{19}$ core for separation by the magnetic field. The photocatalytic activity of the as-prepared magnetic photocatalyst is enhanced with $BaFe_{12}O_{19}$ doping. Besides, the saturation magnetizations of $BaFe_{12}O_{19}$-TiO_2 nanoparticles decreased in comparison to pure hexaferrite, while the coercivity remains almost constant.

Keywords Ceramics · Composite materials · Solid state reaction · Photocatalysis · Magnetic measurements

1 Introduction

During the past decade, hexaferrites presenting the M, Y, and Z-type structures have become important candidates for a variety of commercially magnetic materials since they are magnetically hard, with high coercivity and magnetic permeability, and contain high magnetocrystalline anisotropy along the c-axis of the hexagonal structure. These ferrite magnets are very attractive as they present high magnetization saturation (Ms) as well as high Curie temperature around 450 °C. Besides, these compounds are known by their high magnetocrystalline anisotropy constant. Due to these interesting properties, several elaborating techniques have been developed to obtain a low-production-cost BaM powder specimens. These compounds have been particularly produced by the conventional ceramic method, associating the calcinations of a mixture of $BaCO_3$ and Fe_2O_3 at 1100 °C. An interesting approach consists on doping BaM [1–4] to modify its physical properties, since the core–shell structure composite particles often exhibit improved physical and chemical properties over their single-component counterpart and hence are very useful in a broader range of applications [5, 6].

Besides, anatase-type TiO_2 has attracted much attention for its potential application in the decomposition of various environmental pollutants in both gaseous and liquid phases [7–9]. The photocatalytic degradation systems using fine TiO_2 powder under UV irradiation have been widely investigated [10, 11].

However, in treating pollutants in water, there are at least two obvious problems arising from using fine TiO_2 powders: (1) separation of photocatalysts from the reaction media is difficult and (2) particulate suspensions are not easily applicable to continuous process. An alternative method is immobilizing TiO_2 powders onto an inert and porous supporting matrix such as silica [12] and activated carbon [13–16]. Among them, activated carbon is the most commonly used support for TiO_2 in gas and water treatment due to its porous structure and adsorption properties and the supported catalyst has made remarkable effects in

✉ Wissem Cheikhrouhou-Koubaa
wissem.koubaa@yahoo.fr

1 LT2S Lab Digital Research Center of Sfax Technopark, Sfax/Sfax University, BP 275, 3021 Sfax, Tunisia

2 Lanser Laboratory, Centre de Recherches et des Technologies de l'Energie Technopole Borj Cedria, Bp 95, 2050 Hammamm Lif, Tunisie

3 Université de Rouen, Groupe de Physique des Matériaux GPM UMR 6634 CNRS, UFR Sciences et Techniques, Avenue de l'Université - BP12, 76801 Saint Etienne du Rouvray, France

the kinetics of disappearance of the pollutants, each pollutant being more rapidly photodegraded. This effect has been explained by the adsorption of organics on activated carbon followed by a transfer to the TiO_2 surface where it is immediately degraded. However, activated carbon is usually in the form of granules and powder, and the problem of filtering and recovery still exists. Recently, iron oxide particles have been coated with TiO_2 to synthesize magnetic photocatalytic particles to recover the photocatalyst particles from the treated water stream by magnetic photocatalysts based on Fe_3O_4 doped with TiO_2 or SiO_2, using various heat treatments and a couple of different TiO_2 precursors, that is, titanium butoxide and titanium isopropoxide.

2 Experimental Section

2.1 Fabrication of Pure $BaFe_{12}O_{19}$ and 70% $BaFe_{12}O_{19}$-30%TiO_2 Nanocomposites

The starting materials Fe_2O_3 (≥ 99%, Merck) and $BaCO_3$ (≥ 99%, Merck) powders were mixed in a Fe/Ba molar ratio of 11. It is noted that the stoichiometric molar ratio of Fe/Ba in barium hexaferrite ($BaFe_{12}O_{19}$) is 12; however, using excess barium ions has been recommended in the previous works [17, 18]. Mechanical activation was carried out at four different milling energy levels in a high-energy planetary ball milling with hardened steel vial and balls under air atmosphere. The processed samples were then calcined in air at 800, 1000, and 1100 °C for 2 h with a heating rate of 10 °C/min.

In the next step, 1.5 g of TiO_2 nanopowder (≥ 99%, Sigma-Aldrich) was then added to 5 g of the prepared powder (BaM). Then, the mixture was ground for 90 min at room temperature before being wet mixed. The prepared mixture was dried at 450 °C for 3 h and pressed into pellets of 12-mm diameter and 0.5-cm thickness (with addition of vinyl-alcohol as a binding material) using electric press. The disks were sintered at 700 °C for 3 h. Finally, $BaFe_{12}O_{19}$/TiO_2 was ground to get a powder in good homogenizing and small grain size.

2.2 Characterization of Pure $BaFe_{12}O_{19}$ and 70% $BaFe_{12}O_{19}$-30% TiO_2 Nanocomposite

Characterizations of all samples were carried out with different techniques. Structural properties were determined by X-ray diffraction by the means of an automated Bruker D8 advance X-ray diffractometer with Cu K_α radiations ($\lambda = 1.541$ Å) in 2θ ranging from 20 to 80°. The morphology and particle size of samples were investigated by a scanning electron microscope. Magnetic properties were obtained by using an extraction magnetometer operating between 300 and 800 K.

Optical measurements were deduced from (transmission/reflection) spectra taken from Ultraviolet–visible-near-infrared (UV–VIS-NIR) Perkin Elmer Lambda spectrophotometer in the wavelength range of 200–1200 nm at room temperature.

Finally, photocatalytic activity of the samples was evaluated by the degradation of a standard organic dye: methylene blue (MB), in aqueous solution under visible light irradiation for 2 h. For irradiation, visible modeled sun light was used at the distance of 10 cm from the solution in a dark box.

Since hexaferrites are hard magnetic materials and in order to avoid problems during magnetic agitation, we decide to adhere our powders on glass substrates using a suitable agent.

Typically, 5 ml of MB aqueous solution was placed in a box and photocatalyst films (area of 2×2 cm^2) were put into the solution for each test. Prior to each irradiation, the solution was magnetically stirred in dark for 30 min to promote an adsorption desorption equilibrium. MB decomposition evaluation was carried out using Carry UV–Visible absorption spectroscopy working in a transmission mode, following the MB absorption peak intensity decrease at 660 nm [19].

3 Results and Discussion

3.1 Structural Analysis

Figure 1 illustrates the structure of both pure $BaFe_{12}O_{19}$ and $BaFe_{12}O_{19}$-TiO_2 composite. The XRD pattern of the $BaFe_{12}O_{19}$ powders showed a hexagonal symmetry of pure $BaFe_{12}O_{19}$ and demonstrate the magneto-plumbite structure with no extra reflections. The peaks appeared at $2\theta = 30.32°$, 30.94°, 32.18°, 34.18°, 35.42°, 36.96°, and 56.41° are perfectly indexed to (110), (112), (107), (114), (200), (203), and (2, 0, 11) crystal planes of hexagonal $BaFe_{12}O_{19}$ (PDF# 43–0002). The relative intensities of (107) and (114) peaks, which correspond to the inclined c-axis orientation, are higher than those of (112) and (200) peaks.

These results indicate that the grains of $BaFe_{12}O_{19}$ ceramics are randomly oriented. These peaks are still present in the XRD pattern of $BaFe_{12}O_{19}$-TiO_2 composite, indicating the stability of both compounds during the sintering process. In addition to the presence of other diffraction peaks, those appearing around $2\theta = 25.3°$, 48.0°, 62.1°, 62.7°, and 70.3° were ascribed to the (101), (200), (213), (204), and (220) Bragg reflections of the body-centered tetragonal TiO_2 anatase phase with a fixed volume of 136.313 Å^3 (the JCPDS card number is 21–1272). Conversely, the peaks that appeared at $2\theta = 27.5°$, 36.2°, 41.3°, 44.1°, 54.4°, 56.8°, and 69.2° were ascribed to the (110), (101), (111), (210), (211),

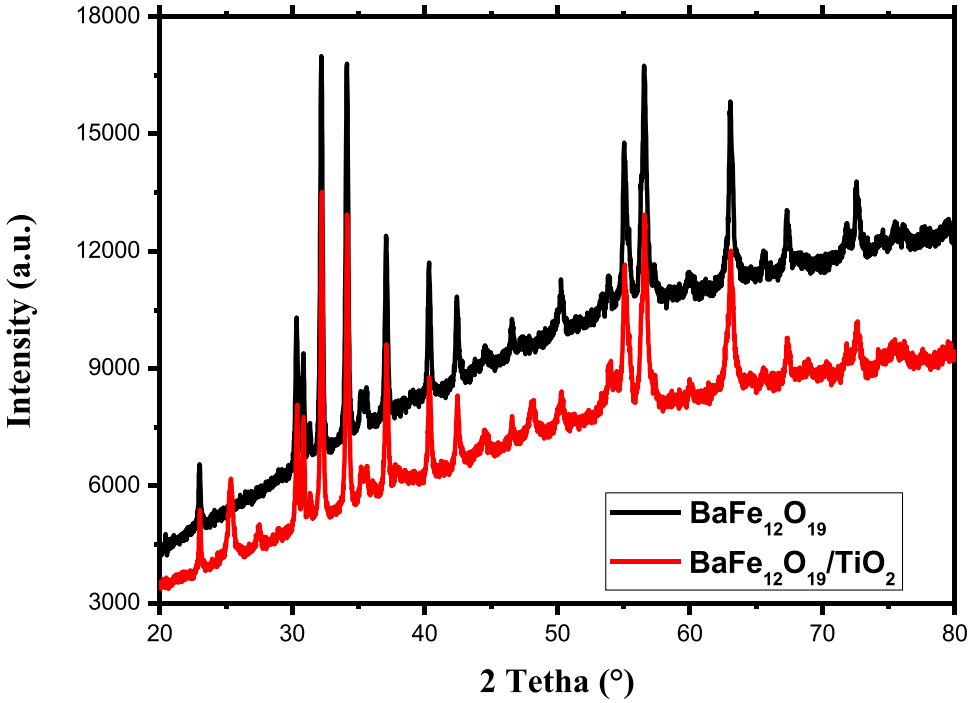

Fig. 1 XRD patterns of pure $BaFe_{12}O_{19}$ and 70% $BaFe_{12}O_{19}$-30% TiO_2 nanocomposite

(220), and (301) Bragg reflections of the primitive tetragonal TiO_2 rutile phase with a fixed volume of 62.0516 $Å^3$ (JCPDS card number is 89–4920).

3.2 Morphology

The morphology and particle size of samples were investigated using a scanning electron microscope (Fig. 2). It can be seen that the structure of $BaFe_{12}O_{19}$ is hexagonal and the average particle size is estimated to be in the range of 200 nm. A slight agglomeration was also observed, which is due to the high surface energy and the magnetic interactions of the nanoparticles.

3.3 Magnetic Properties

The magnetic properties of pure $BaFe_{12}O_{19}$ and $BaFe_{12}O_{19}$-TiO_2 nanocomposites are shown in Fig. 3. The magnetic parameters such as saturation magnetization (Ms), coercivity (Hc), and remnant magnetization (Mr) are given in Table 1. It can be clearly seen that the value of saturation magnetization decreases with TiO_2 doping. It is mainly

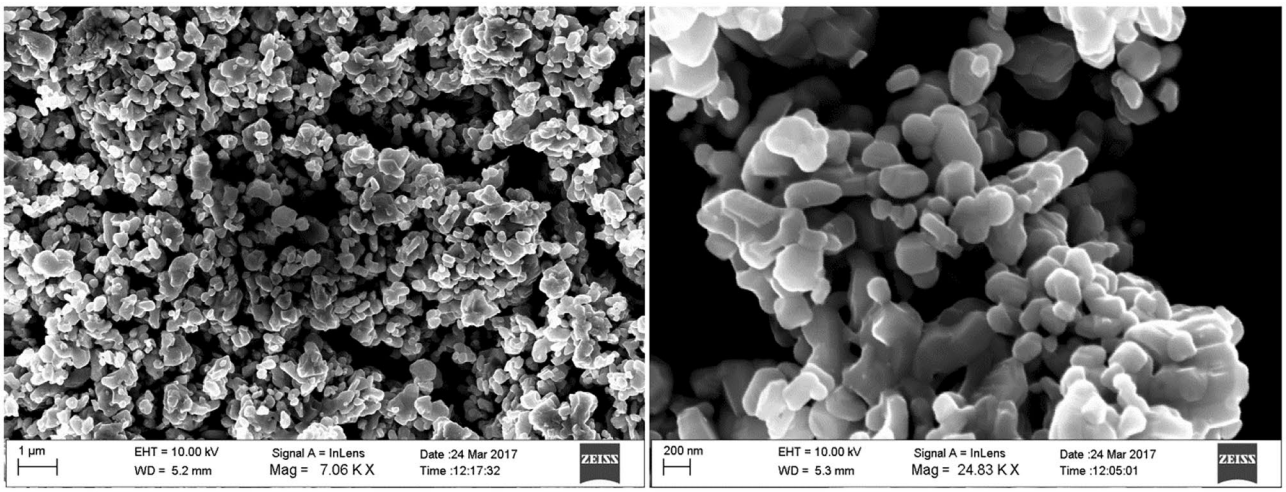

Fig. 2 SEM photographs of barium ferrite ceramics

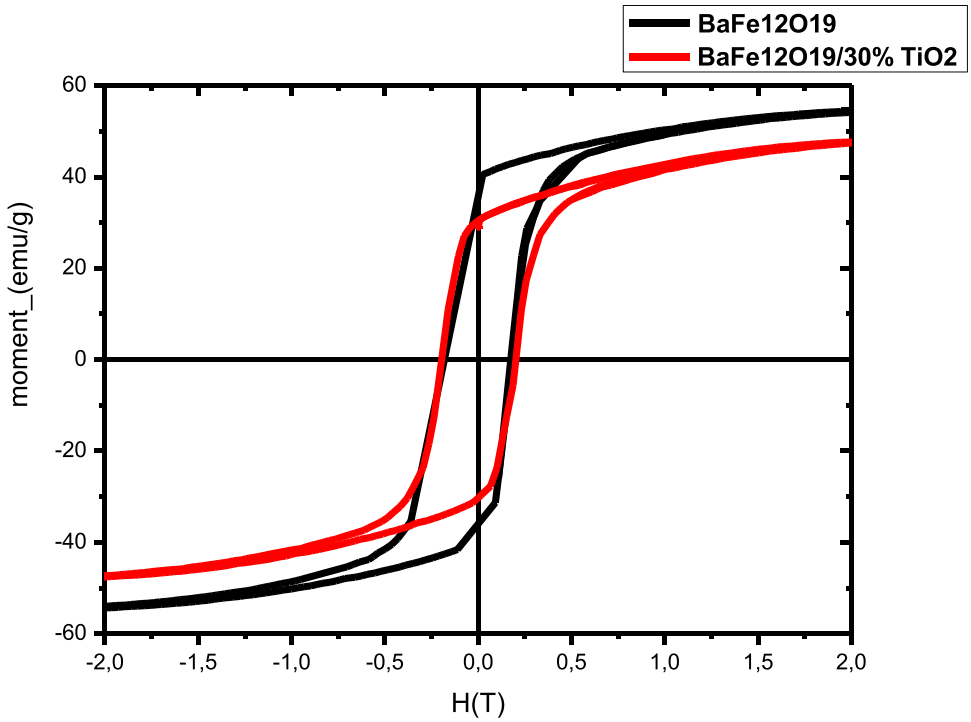

Fig. 3 Hysteresis loops at room temperature for pure $BaFe_{12}O_{19}$ and 70% $BaFe_{12}O_{19}$-30% TiO_2 nanocomposite

attributed to the contribution of the non-magnetic component to the total magnetization. In fact, the non-magnetic particles can be considered as a magnetically dead component for the composite, which induces a decrease of the magnetization. However, the coercivity of both compounds remains constant as it represents the property of a magnetic material and is determined by the strength of magnetic dipoles in the magnetic domains as well as the relations between adjacent magnetic domains.

Note that, although the particles are nanoscale, they are not super-paramagnetic as confirmed from the high H_C values.

In general, the ferrite materials that hold high coercivity values are called "hard ferromagnetic" materials and these compounds embrace good magnetic properties which have a very good stability against magnetic property losses. The obtained coercivity proved that the prepared barium ferrite–supported TiO_2 is an excellent ferromagnetic material. Thus, the prepared supported photocatalyst can be almost completely recovered with minimum loss, for many numbers of cycles with no diminishing in both the magnetic property and photoactivity.

Table 1 Magnetic property of pure $BaFe_{12}O_{19}$ and 70% $BaFe_{12}O_{19}$-30% TiO_2 nanocomposite

Sample	M_S (emu/gr)	H_C (T)	Mr (emu/gr)
100% $BaFe_{12}O_{19}$	54.62	0.2	40.35
70% $BaFe_{12}O_{19}$/30% TiO_2	47	0.2	30

3.4 Magnetic Measurements at Low Field H = 0.05 T

Magnetization measurements versus temperature were also carried out for our compounds at high temperatures, typically between 300 and 800 K, under 0.05 T (Fig. 4).

We clearly observe a ferromagnetic–paramagnetic transition as the temperature increases. Note that the magnetization has decreased in the composite with 30% TiO_2; this result is expected since the titanium oxide is non-magnetic, and its role is to dilute the grain boundaries in the composite, which causes the reduction of the magnetic response.

It should be noted that the value of the Curie temperature (T_C) for each sample was determined from the inflection point at the level of the thermomagnetic curve M (T), by plotting the minimum of dM (T)/dT.

Note that the transition point was not affected by the doping with titanium oxide. The Curie temperature is approximately 727 K for both compounds (Fig. 5).

3.5 Optical Study

Optical absorption on semiconductor materials is an important factor in photocatalytic efficiency, since a narrow band gap results in high absorption efficiency of solar spectrum photons. The UV–visible spectra of $BaFe_{12}O_{19}$ and $BaFe_{12}O_{19}/TiO_2$ are presented in Fig. 6.

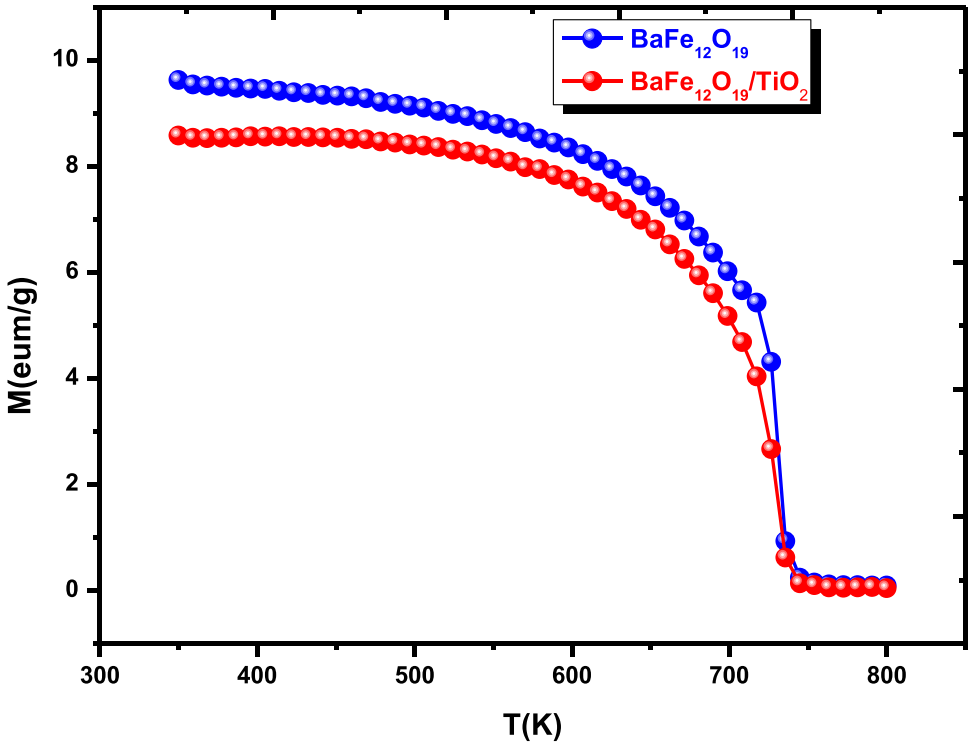

Fig. 4 Thermal variation of the magnetization M (T) for the two compounds $BaFeO_{19}$ and BaFeO19/TiO2 under a magnetic field of 0.05 T

The energy band gap of the as-deposited samples was calculated from the following relation [20]:

$$\alpha h\nu = A(h\nu - Eg)^{n/2}$$

where ν is the absorption coefficient, $h\nu$ is the photon energy, A is a constant for transition, and E_g is the band gap of the semiconductor. The n value depends on the optical transition type of semiconductors, e.g., $n=1$ for direct transition, and $n=4$ for indirect transition. As reported in the literature, both $BaFe_{12}O_{19}$ and TiO_2 are indirect transition semiconductors [21, 22]. Therefore, as illustrated in Fig. 7, the band-gap energy (E_g) of the samples has been determined by

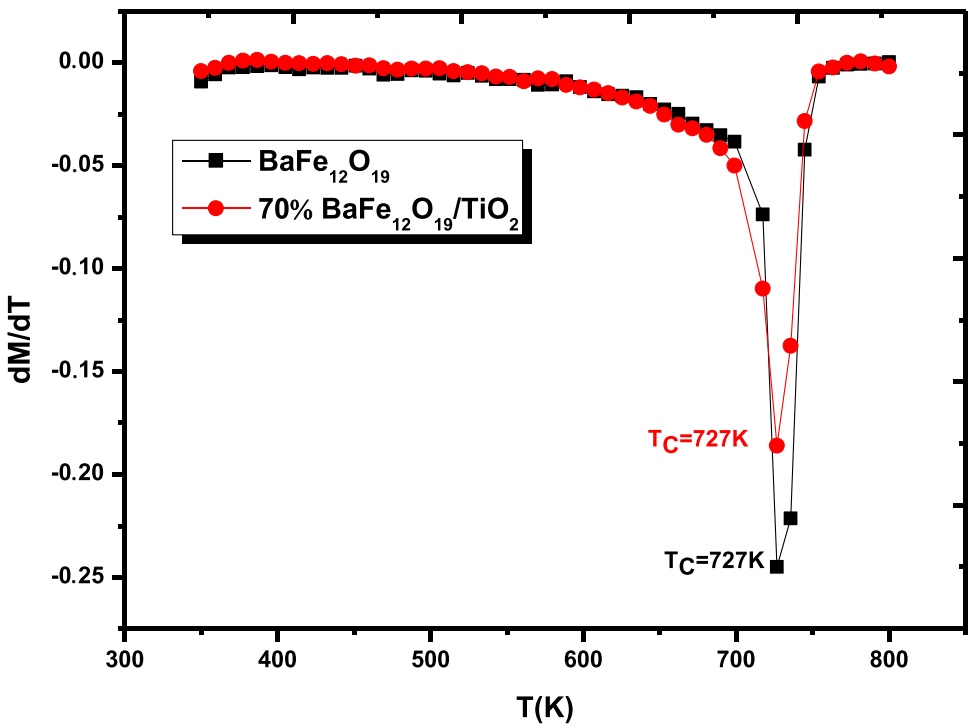

Fig. 5 The variations of the Curie temperature T_C as a function of the TiO_2 content of the compounds $BaFeO_{19}$ and $BaFeO_{19}/TiO_2$

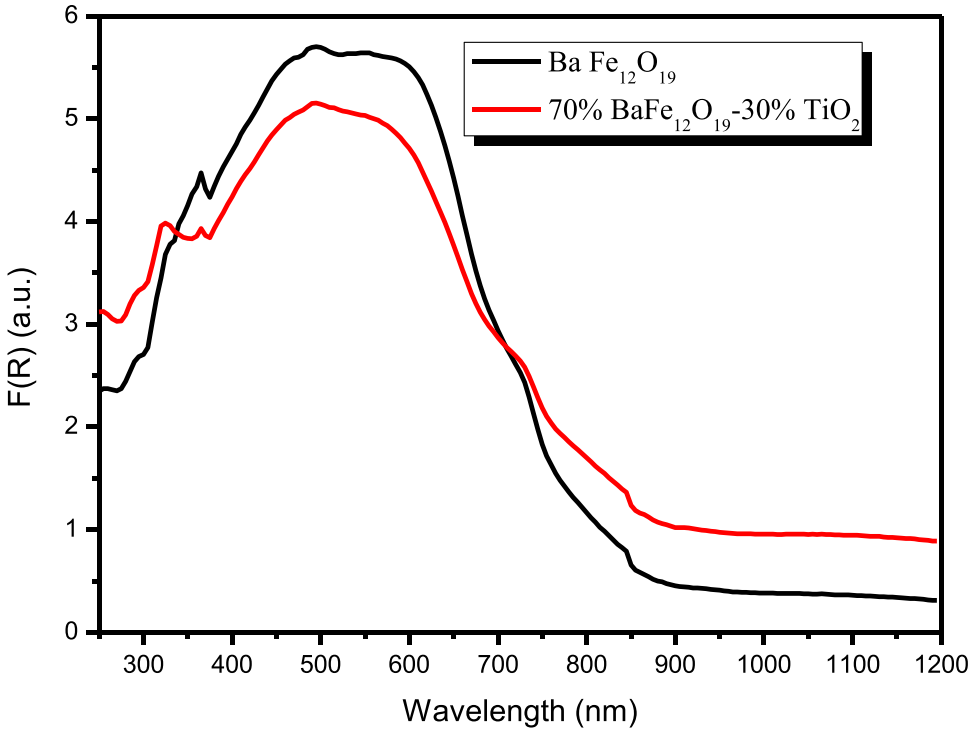

Fig. 6 UV–Visible absorption spectra of pure $BaFe_{12}O_{19}$ and 70% $BaFe_{12}O_{19}$-30% TiO_2 nanocomposite

extrapolating the linear portion of the plots of $(\alpha h\nu)^2$ versus photon energy ($h\nu$) to the energy axis. The estimated band gap energy of $BaFe_{12}O_{19}$ and $BaFe_{12}O_{19}/TiO_2$ was 1.74 eV and 1.71 eV, respectively, which implies that both samples can be activated with visible light photons of wavelengths lower than the absorption edge wavelength.

3.6 Photocatalytic Activities

As previously explained in the "Experimental Section" section, MB solution was chosen as a polluent model to evaluate the photocatalytic efficiency of the prepared photocatalysts. Visible absorption spectra recorded on the MB

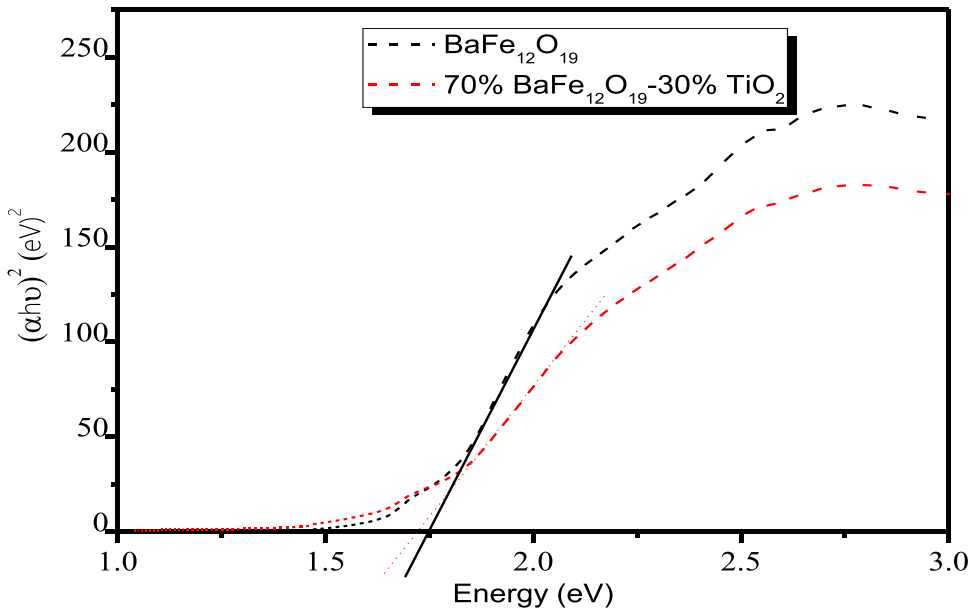

Fig. 7 The estimated band gap energy of $BaFe_{12}O_{19}$ and $BaFe_{12}O_{19}/TiO_2$

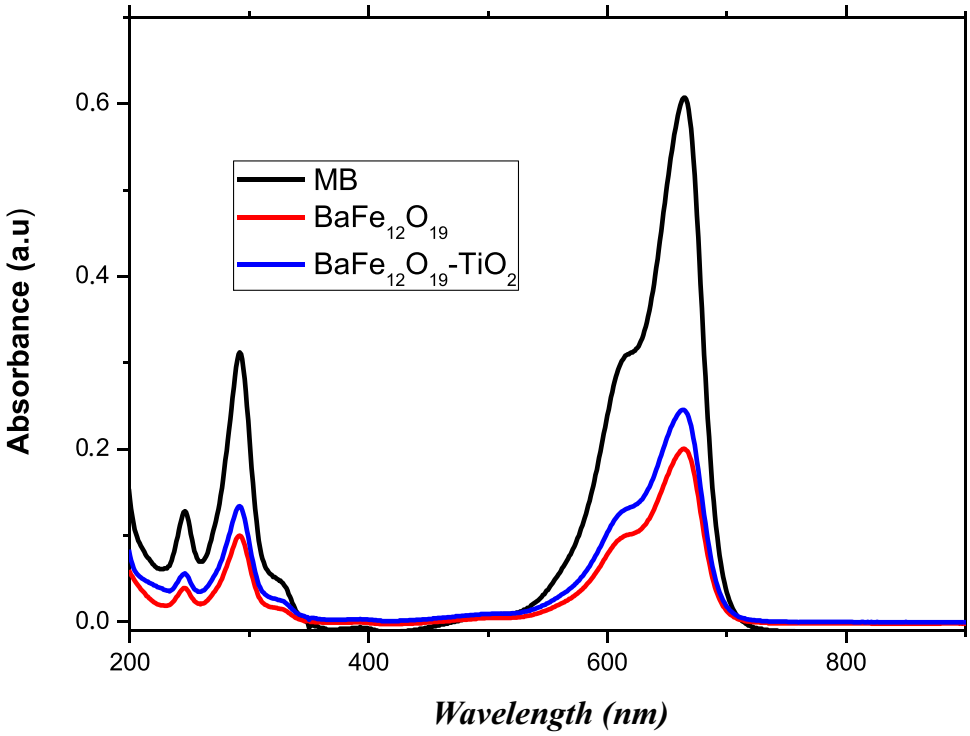

Fig. 8 The photodegradation of the MB of pure $BaFe_{12}O_{19}$ and 70% $BaFe_{12}O_{19}$-30% TiO_2 nanocomposite photocatalyst under visible irradiation

aqueous solution before and after contact with photocatalyst samples are given in Fig. 8.

Clearly, the $BaFe_{12}O_{19}$ nanopowder presents higher intrinsic activity for the photodegradation of the MB in the visible range. This activity is demonstrated by the considerable decrease in the absorbance at 660 nm. Although TiO_2 is the most suited compound to photocatalysis [23–28] under UV–visible range, it does not work in the visible field which makes $BaFe_{12}O_{19}$ the most suitable photocatalyst (Fig. 9).

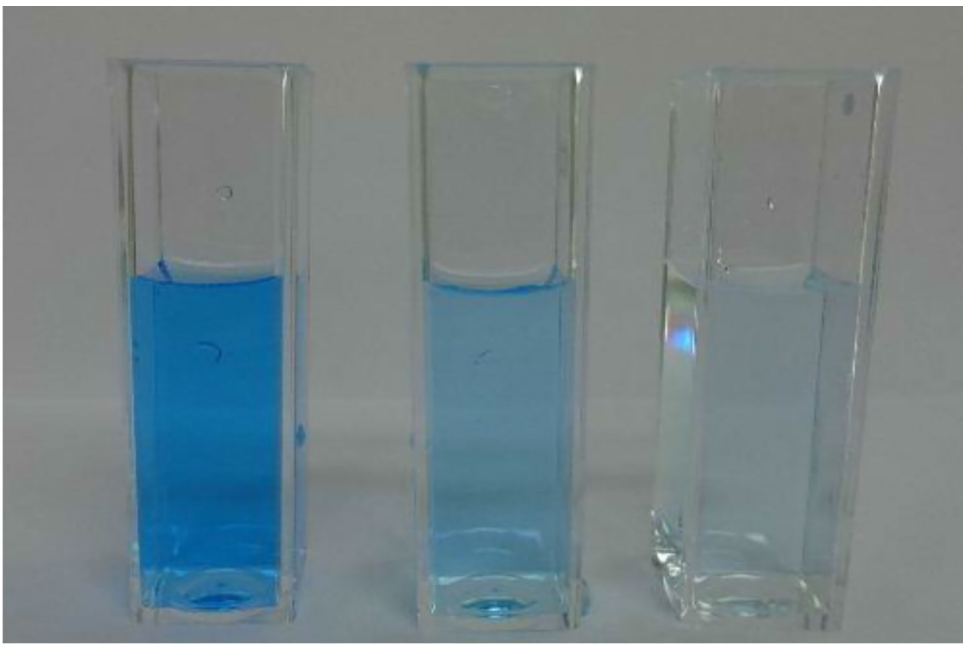

Fig. 9 MB final solution photograph obtained by MB, 70% $BaFe_{12}O_{19}$-30% TiO_2 nanocomposite, and pure $BaFe_{12}O_{19}$ photocatalyst under visible irradiation

4 Conclusions

The photocatalysis effect of TiO_2-supported $BaFe_{12}O_{19}$ on the degradation of (MB) was successfully studied. The supported photocatalysts exhibited an enhanced structural, in addition to its magnetic properties, as well as photocatalytic process under visible light irradiation. A higher degradation of MB was achieved. This has not been reported previously.

The results of the presently prepared photocatalysts supported on barium ferrite laid a pathway for a green and sustainable catalyst design.

Thus, the TiO_2-$BaFe_{12}O_{19}$ photocatalyst could serve as a new generation of photocatalyst for the complete, economical, and productive treatment of toxic wastewater without losing its important magnetic properties.

Acknowledgements This work has been supported by the Tunisian Ministry of Higher Education and Scientific Research.

References

1. Pawar, R.A., Desai, S.S., Tamboli, Q.Y., Shirsath, S.E., Patange, S.M.: J. Magn. Magn. Mater. **378**, 59 (2015)
2. Singh, V.P., Kumar, G., Kotnala, R.K., Shah, J., Sharma, S., Daya, K.S., Batoo, K.M., SinghJ, M.: Magn. Magn. Mater. **378**, 478 (2015)
3. Remya, K.P., Prabhu, D., Amirthapandian, S., Viswanathan, C., Ponpandian, N.: J. Magn. Magn. Mater. **406**, 233 (2016)
4. Yang, H.B., Liu, M., Lin, Y., Dong, G.Q., Hu, L.Y., Zhang, Y., Tan, J.Y.: Mater. Chem. Phys. **160**, 5 (2015)
5. Fu, W., Yang, H., Chang, L., Li, M., Bala, H., Yu, Q., Zou, G.: Colloids Surf. A Physicochem. Eng. Asp. **71**, 262 (2005)
6. Mayya, K.S., Gittins, D.I., Caruso, F.: Chem. Mater. **13**, 3833 (2001)
7. Li, G., Gray, K.A.: Chem. Phys. **339**, 173 (2007)
8. Toyoda, M., Nanbu, Y., Nakazawa, Y., Hirano, M., Inagaki, M.: Appl. Catal. B Environ. **49**, 227 (2004)
9. Kolen'ko, Y.V., Churagulov, B.R., Kunst, M., Mazerolles, L., Colbeau-Justin, C.: Appl. Catal. B Environ. **54**, 51 (2004)
10. Hoffmann, M.R., Martin, S.T., Choi, W., Bahnemann, D.W.: Chem. Rev. **95**, 69 (1995)
11. Hidaka, H., Zhao, J., Pelizzetti, E., Serpone, N.: J. Phys. Chem. **96**, 2226 (1992)
12. Ilisz, I., András, D., Károly, M., Dékány: Colloids Surf. A Physicochem. Eng. Asp. **230**, 89 (2004)
13. Matos, J., Laine, J., Herrmann, J.M.: J. Catal. **200**, 10 (2001)
14. Ao, C.H., Lee, S.C.: J. Photochem. Photobiol. A Chem. **161**, 131 (2004)
15. Tsumura, T., Kojitani, N., Umemura, H., Toyoda, M., Inagaki, M.: Appl. Surf. Sci. **196**, 429 (2002)
16. Herrmann, J.M., Matos, J., Disdier, J., Guillard, C., Laine, J., Malato, S., Blanco, J.: Catal. Today **54**, 255 (1999)
17. Mali, A., Ataie, A.: J. Alloys Comp. **399**, 245 (2005)
18. Wang, L., Zhang, Q.: J. Alloys Comp. **469**, 251 (2009)
19. Ben Naceur, J., Gaidi, M., Bousbih, F., Mechiakh, R., Chtourou. R.: Current applied physics **12**, 422 (2012)
20. Kuang, P. -Y., Zheng, P. -X., Liu, Z. -Q., Lei, J. -L., Wu, H., Li, N., et al.: Embedding Au quantum dots in rimous cadmium sulfde nanospheres for enhanced photocatalytic hydrogen evolution. Small. 02870 (2016)
21. Monllor-Satoca, D., Gomez, R., González-Hidalgo, M., Salvador, P.: The, "Diret-Indirect" model: an alternative kinetic approach in heterogeneous photocatalysis based on the degree of interaction of dissolved pollutant species with the semiconductor surface. Catal Today **129**, 247–255 (2007)
22. Karmakar, M., Mondal, B., Pal, M., Mukherjee, K.: Acetone and ethanol sensing of barium hexaferrite particles: a case study considering the possibilities of non-conventional hexaferrite sensor. Sens. Actuators, B. **190**, 627 (2014)
23. Chioma Affam, A., Chaudhuri, M.: J. Environ. Manag. **130**, 160 (2013)
24. Prasad, G.K., Ramacharyulu, P.V.R.K., Kumar, J.P., Srivastava, A.R., Singh, B.: Thin Solid Films **520**, 5597 (2012)
25. Lee, S.Y., Park, S.J.: J. Ind. Eng. Chem. **19**, 1761 (2013)
26. Lazar, M.A., Varghese, S., Nair, S.S.: Catalysts **2**, 572 (2012)
27. Savio, A.K.P.D., Fletcher, J., Robles Hernández, F.C.: Ceram. Int. **39**, 2753 (2013)
28. Savio, A., Fletcher, J., Robles Hernández, F.: Ceram. Int. **39**, 2753 (2013)

Publisher's Note Springer Nature remains neutral with regard to jurisdictional claims in published maps and institutional affiliations.

Springer Nature or its licensor holds exclusive rights to this article under a publishing agreement with the author(s) or other rightsholder(s); author self-archiving of the accepted manuscript version of this article is solely governed by the terms of such publishing agreement and applicable law.